Full latitudinal marine atmospheric measurements of iodine monoxide

Hisahiro Takashima[1,2], Yugo Kanaya[2], Saki Kato[1], Martina M. Friedrich[3],

Michel Van Roozendael[3], Fumikazu Taketani[2], Takuma Miyakawa[2], Yuichi Komazaki[2],

Carlos A. Cuevas[4], Alfonso Saiz-Lopez[4], and Takashi Sekiya[2]

[1] Faculty of Science, Fukuoka University, Fukuoka, Japan

[2] Japan Agency for Marine–Earth Science and Technology (JAMSTEC), Yokohama, Japan

[3] Belgian Institute for Space Aeronomy (BIRA-IASB), Brussels, Belgium

[4] Department of Atmospheric Chemistry and Climate, Institute of Physical Chemistry Rocasolano (CSIC), Madrid, Spain

Correspondence to: Hisahiro Takashima (hisahiro@fukuoka-u.ac.jp) and Yugo Kanaya (yugo@jamstec.go.jp)

Abstract. Iodine compounds destroy ozone (O_3) in the global troposphere and form new aerosols, thereby affecting the global radiative balance. However, few reports have described the latitudinal distribution of atmospheric iodine compounds. This work reports iodine monoxide (IO) measurements taken over unprecedented sampling areas from the Arctic to the Southern Hemisphere and spanning sea surface temperatures (SSTs) of approximately 0°C to 31.5°C. The highest IO concentrations were observed over the Western Pacific warm pool (WPWP), where O_3 minima were also measured. There, negative correlation was found between O_3 and IO mixing ratios at extremely low O_3 concentrations. This correlation is not explained readily by the "O_3-dependent" oceanic fluxes of photolabile inorganic iodine compounds, the dominant source in recent global-scale chemistry-transport models representing iodine chemistry. Actually, the correlation rather implies that "O_3-independent" pathways can be similarly important in the WPWP. The O_3-independent fluxes result in a 15% greater O_3 loss than that estimated for O_3-dependent processes alone. The daily O_3 loss rate related to iodine over the WPWP is as high as approximately 2 ppbv despite low O_3 concentrations of approximately 10 ppbv, with the loss being up to 100% greater than that without iodine. This finding suggests that warming SST driven by climate change might affect the marine atmospheric chemical balance through iodine–ozone chemistry.

1 Introduction

Halogens play an important role in tropospheric and stratospheric chemistry through the catalytic destruction of ozone (O_3), which affects the atmosphere's oxidizing capacity and the radiative balance of the Earth (Alicke et al., 1999; Koenig et al.,

30 2020; Read et al., 2008; Saiz-Lopez et al., 2012; Saiz-Lopez et al., 2014; Simpson et al., 2015). Iodine, particularly is potentially important in tropospheric chemistry because of its rapid reactions, although its concentration in the troposphere is low compared to that of chlorine and bromine. Iodine also forms aerosol particles; it can thereby affect the global radiative balance (O'Dowd et al., 2002; Sipila et al., 2016; Gómez-Martín et al., 2020; Baccarini et al., 2020; Gómez-Martín et al., 2021; He et al., 2021).

35   Because of their low concentrations in the atmosphere, iodine compounds are difficult to quantify. Few reports have attempted to clarify their regional to global-scale sources and roles in atmospheric chemistry (Großmann et al., 2013; Mahajan et al., 2012; Prados-Roman et al., 2015a; Dix et al., 2013; Volkamer et al., 2015). In the past, the primary source of iodine in the troposphere has long been regarded as organic compounds in coastal areas (Davis et al., 1996; Carpenter et al., 2012; Prados-Roman et al., 2015a). However, results of recent studies suggest that iodine compounds over the open ocean are emitted

40 from inorganic sources following O_3 deposition over the ocean surface (Carpenter et al., 2013; Macdonald et al., 2014; Prados-Roman et al., 2015a). The inorganic sources are now regarded as the dominant emission term over the oligotrophic oceans in the global-scale chemistry-transport models representing iodine chemistry (e.g., Saiz-Lopez et al., 2014; Sekiya et al., 2020), although the emission process of inorganic iodine is still insufficiently clear in more recent studies (e.g., Inamdar et al., 2020).

This study specifically examines iodine monoxide (IO) in the marine boundary layer over the open ocean from the wide

45 latitudinal bands. Specifically, we examine processes occurring over the tropical western Pacific, where the global sea surface temperature (SST) reaches a maximum (warm pool) and where O_3 minima have been reported (Rex et al., 2014; Kanaya et al., 2019; Kley et al., 1996). Actually, IO observations in environments with SSTs of >30°C are limited. Observations of IO have been made in the tropics, but only for short time periods with SST > 30°C, if any (Großmann et al., 2013; Dix et al., 2013; Prados-Roman et al., 2015a). Although the importance of halogen chemistry as a driver of O_3 losses in this region has been

50 suggested (Großmann et al., 2013; Koenig et al., 2017), this point has yet to be examined in the context of full latitudinal distributions.

The initial production of atmospheric inorganic iodine species has not been fully examined in an environment where extremely low O_3 concentrations (<10 ppb) are observed. Over the Atlantic Ocean (in Cape Verde), long-term observations of iodine and ozone have been conducted, but they were in higher O_3 environments of approximately 20 ppbv (Read et al., 2008).

55 We therefore examined IO variations over the tropical western Pacific and their potential contributions to regional O_3 losses, with emphasis on SST as a potential key parameter controlling the initial iodine emissions. The global SST maximum is observed in the tropical western Pacific, but observations reported from earlier studies were only taken in the regions surrounding the maximum (Großmann et al., 2013; Prados-Roman et al., 2015a). Investigation of iodine variations in the tropics is also important for elucidating the stratospheric chemical balance (Koenig et al., 2017) because transport from the

60 troposphere to the stratosphere occurs through the Tropical Tropopause Layer (Takashima et al., 2008; Saiz-Lopez et al., 2015; Koenig et al., 2017; Holton et al., 1995). In fact, it is particularly important over the tropical western Pacific.

For this study, using the multi-axis differential optical absorption spectroscopy (MAX–DOAS) remote sensing technique, IO observations were made to quantify IO concentrations over the open ocean, covering the widest latitudinal range ever

examined with a single instrument. The technique uses scattered solar radiation at several elevation angles to obtain
65 atmospheric aerosol and gas profile concentrations (Hönninger et al., 2004; Wagner et al., 2004; Wittrock et al., 2004; Sinreich et al., 2005; Frieß et al., 2006; Kanaya et al., 2014). MAX–DOAS generally measures trace-gas contents over a long light path (up to 10–20 km) at low elevation angles. The long light path enables the detection of low concentrations of species of interest at near-surface altitudes. MAX–DOAS is therefore useful for quantifying low-abundance tropospheric trace gases such as IO over the open ocean.

70 Multi-platform measurements by MAX–DOAS from aircraft (Koenig et al., 2017; Volkamer et al., 2009) and ships (Großmann et al., 2013; Takashima et al., 2012; Volkamer et al., 2009) have been developed in recent years. Earlier studies have retrieved IO concentrations (typically < 1 pptv) in the marine boundary layer over the open ocean from shipboard MAX–DOAS measurements (Großmann et al., 2013; Mahajan et al., 2012; Prados-Roman et al., 2015a; Inamdar et al., 2020). Since 2008, the Japan Agency for Marine–Earth Science and Technology (JAMSTEC) has undertaken an unprecedented set of
75 MAX–DOAS measurements on board the research vessels (R/Vs) *Kaiyo*, *Mirai*, and *Kaimei* around the world (Takashima et al., 2012). This report presents IO and O_3 variations over the open ocean from the Arctic to the Southern hemisphere observed on RV *Mirai* between 2014–2018.

2 Methodology

2.1 Iodine monoxide observations from ship-based MAX–DOAS measurements

80 The shipboard MAX–DOAS apparatus used for this study comprised two main components: an outdoor telescope and an indoor UV–Vis spectrometer (SP-2358; Acton Research Corp., coupled to a PIXIS-400B back-illuminated CCD detector; Teledyne Princeton Instruments). These were connected using a 10–14 m long fiber-optic cable (100 µm radius, 60-core or 40-core). The telescope unit was developed jointly by the Japan Agency for Marine–Earth Science and Technology (JAMSTEC) and PREDE Co. Ltd. (Tokyo, Japan). The movable prism of the telescope unit rotates for elevation angles (ELs)
85 of 3°, 5°, 10°, 30°, and 90°. The EL is changed every minute to observe scattered sunlight. The target EL is attained by adjusting the angle of the prism actively, and by considering the angle of the ship's roll (Takashima et al., 2016). The telescope line-of-sight was off the starboard side of the ship with a field of view of approximately 1.0°. The spectrometer was housed in an adiabatic plastic box with the temperature held constant at 35°C ± 0.1°C using a temperature controller (KT4; Panasonic Inc., Japan). The CCD was cooled to −70°C. The spectrometer was equipped with a 600 line mm^{-1} grating at 300 nm. The slit width
90 was 100 µm. The typical exposure time was 0.1–0.2 s.

Spectral data were selected for analysis when the EL was within ±0.5°of the target. Data were analyzed using the DOAS method (Platt and Stutz, 2008). A nonlinear least-squares spectral fitting procedure was used to derive differential slant column densities (DSCDs) of the oxygen collision complex (O_2–O_2 or O_4) and IO using the QDOAS software package (Danckaert et al., 2017), for which absorption cross-section data presented in Table 1 were used. For O_4 and IO retrievals, 425–490 nm and
95 415–438 nm fitting windows were applied, respectively. Examples of fitting results and the time series of DSCDs are presented

respectively in Figures 1 and 2. The typical fitting error of the IO DSCDs was approximately 1×10^{12} molecules cm^{-2}, with a detection limit of approximately 4×10^{12} molecules cm^{-2} (2σ).

The Mexican Maxdoas Fit (MMF) retrieval algorithm (Friedrich et al., 2019) was used for retrieval of IO profiles and vertical column densities. The version of MMF used in this study is the same as used in Frieß et al. (2019) and Tirpitz et al. (2021) but with adjusted a priori and variance-covariance matrix settings to fit for IO retrieval. MMF applies the optimal estimation method and uses a two-step approach in which the aerosol profile is first retrieved from O_4 DSCDs. Then, the IO profile is retrieved from the IO DSCDs using the earlier retrieved aerosol profile in the forward model. We used VLIDORT (v.2.7) (Spurr, 2006) as the forward model in a pseudo-spherical multiple-scattering setting. Only intensity information and its analytically calculated Jacobians were used. No other Stokes parameter was used. MMF was used in logarithmic retrieval space on a retrieval grid of up to 4 km with 200 m layer height.

Both *a priori* profiles were constructed as constant below 500 m with an exponentially decreasing profile above 500 m for aerosol and IO profiles to examine near-surface areas specifically. The *a priori* aerosol optical depth was set as 0.18. The *a priori* IO vertical column density (VCD) was set to 2.5×10^{12} molecules cm^{-2}. The *a priori* covariance matrix **Sa** for both aerosol and IO retrieval was constructed using the square of 100% of the *a priori* profile on the diagonal and a correlation length of 200 m. For the aerosols, the only retrieved quantity was the partial aerosol optical depth per layer. Therefore, in the forward model, a constant single scattering albedo of 0.95 was used for both retrievals: aerosol and IO. The phase function moments were constructed using the Henyey–Greenstein phase function (Henyey and Greenstein, 1941) with a constant asymmetry factor of 0.72. The surface albedo in the forward models was set as 0.06. Here, the single scattering albedo, asymmetry factor, and surface albedo were used similarly to work presented by Großmann et al. (2013). The degrees of freedom (DOFs) for the IO retrieval for MR14-06 (leg1) were 1–1.4. It is also noteworthy that the observed IO contents might be a little low compared with those from earlier studies conducted over the open ocean because of inaccuracy of the water–vapor cross-section used in earlier retrievals (Lampel et al., 2015).

2.2 Zero-dimensional photochemical box model with iodine chemistry

A zero-dimensional photochemical box model (Kanaya et al., 2007a; Kanaya et al., 2007b) based on the Regional Atmospheric Chemistry Mechanism (RACM) (Stockwell et al., 1997) and custom iodine chemistry was updated to include 91 chemical species and 275 reactions (reactions of iodine chemistry added to RACM are presented in Table 3). It was used to simulate the time evolution of mixing ratios of O_3 (initially 18 ppbv) and iodinated species in the boundary layer with assumed height of 500 m over the equatorial Pacific region, where the maximum concentrations of IO and minimum concentrations of O_3 were observed. For O_3, dry deposition at a velocity of 0.04 cm s^{-1} was considered (Pound et al., 2020). Entrainment flux of 1.2×10^8 molecules cm^{-2} s^{-1} was assumed for NO_2, for which the initial mixing ratio was assumed to be 15 pptv. Fluxes of hypoiodous acid (HOI) and I_2 from the ocean surface were estimated respectively (Carpenter et al., 2013) as 8.4×10^7 and 2.6×10^6 molecules cm^{-2} s^{-1} at 10 ppbv of O_3, for an aqueous I$^-$ concentration of 74 nM and wind speed of 5 m s^{-1} (8.9×10^7 molecules cm^{-2} s^{-1} as total HOI/I_2 (= HOI + 2I_2) flux). The I$^-$ concentration was referred from the nearest observation data at

12°N and 158°E (Tsunogai and Henmi, 1971). The assumed wind speed was from observations made during MR14-06 cruise over the region. For Case 1a, the fluxes were assumed to be linearly dependent on O_3, which is consistent with Carpenter et al. (2013). For Case 1b a 25% reduction of the flux was assumed, potentially because of the presence of sea-surface microlayer or dissolved organic matter (Hayase et al., 2010; Hayase et al., 2012; Shaw and Carpenter, 2013; Tinel et al., 2020). The blue band of Figure 3 represents the range of Cases 1a and 1b, representing the case with "O_3-dependent" fluxes. In Cases 2a and 2b, the O_3-dependent flux in Case 1a was reduced to half and compensated by "O_3-independent" inorganic iodine fluxes of 3.3 (or 6.6) $\times 10^7$ molecules cm^{-2} s^{-1} (red band of Figure 3, representing the "quasi-O_3-dependent" case). As a reference, a hypothetical case (Cases 3a and 3b) with purely "O_3-independent" flux of the magnitude of 9.9 (or 13) $\times 10^7$ molecules cm^{-2} s^{-1} was also tested (orange band of Figure 3, representing the "purely O_3-independent" case). The time-dependent simulations continued for five days with evaluation of the mixing ratio of O_3 and its relation with IO involving daytime averages (0600–1800 ship local time) over the first to fourth days. Dry deposition velocities of iodine species (I, IO, HI, HOI, OIO, I_2O_2, INO, INO_2, $IONO_2$, and I_2) were assumed to be 1 cm s^{-1}.

2.3 Backward trajectory calculation

The origins of airmasses over the tropical western Pacific were investigated using five-day backward trajectory calculations (Takashima et al., 2011) based on meteorological analysis data of the European Centre for Medium-range Weather Forecasts (ECMWF).

2.4 In situ gas measurements

For measurements of O_3 and CO, ambient air was sampled using approximately 20 m of Teflon tubing (6.35 mm outer diameter) from the bow (Kanaya et al., 2019). To avoid contamination from ship exhaust, 1-min data deviated more than 1σ from the hourly discrete average were deleted. The typical magnitude of 1σ over the remote ocean was approximately 0.1–0.5 ppbv. The O_3 and CO concentrations were measured respectively using UV and infrared absorptions with O_3 and CO monitors (49C and 48C; Thermo Scientific, USA). The O_3 instrument was calibrated twice per year in the laboratory, before and after deployment, using a primary standard O_3 generator. The CO instrument was calibrated on board twice per year, on embarking and disembarking of the instrument, using a premixed standard gas. The reproducibility of the calibration was to within 1% for O_3 and 3% for CO (Kanaya et al., 2019). The O_3 concentrations observed from the R/V *Mirai* cruises presented in Table 3 are shown in Figure S1.

3 Results and Discussion

The IO contents (differential slant column densities (DSCDs) for an elevation angle of 3°) observed from the R/V *Mirai* during seven research cruises during 2014–2018 are presented in Figure 4. The cruises are presented in Table 3. Although observations were limited to some seasons and years (e.g., Arctic measurements were limited to the Northern Hemisphere summer), whole

latitudinal bands were covered from 74°N to 67°S, and strong latitudinal variations of IO concentrations were observed, with
160 a maximum detected clearly in the tropics (10°S – 10°N), but not at higher latitudes in either hemisphere. Over Southeast Asia (near Indonesia), high IO concentrations were sometimes observed near coastal areas. The highest values of up to approximately 2×10^{13} molecules cm^{-2} (DSCD) were also observed in the tropical western Pacific, with wide variations at global SST maxima (>30°C). From similar earlier studies (Gómez-Martín et al., 2013; Großmann et al., 2013; Mahajan et al., 2012) no data obtained under very high SST conditions over a long period were reported. Therefore, our IO observations at
165 SST maxima (up to 31.5°C) and during more than two weeks represent the most comprehensive measurements of reactive iodine over the tropical Western Pacific warm pool (WPWP).

Specifically regarding IO variations over the tropical western Pacific, we found IO VCDs of approximately 0.7–1.8 $\times$ 10^{12} molecules cm^{-2} (Figure 5). Five-day backward trajectories indicate that air masses in this region originated from the open ocean (Figure 5). The carbon monoxide (CO) content was constantly low (60 ppbv, Figure 6), which is also consistent with an
170 air mass originating from the open ocean. In addition, the chlorophyll content, based on satellite MODIS measurements (NASA Level-3 ver. 2018) in the source region, was also low (Figure 5), implying that any organic source of iodine can be expected to be negligible (although we also must consider abiotic organic source as well as mesotrophic conditions (Jones et al., 2010)). The IO data collected over the tropical western Pacific are consistent with I$^-$ variations reported in earlier studies (Chance et al., 2014; Chance et al., 2019; Sherwen et al., 2016), indicating an increase of I$^-$ concentration with SST.

175 For the time series of IO concentrations near the ocean surface (0–200 m height, Figure 7), the values were approximately 0.3–0.8 pptv, with wide variations over a timescale of a few days. The IO concentration near the surface depends on the shape of the *a priori* profile used for the retrieval, but day-to-day variations near the surface were unaffected by the choice of profile. Insufficient data were retrieved to document diurnal IO variations accurately. At times, the O$_3$ concentrations were generally low (<20 ppbv) and extremely low (<10 ppbv) (Figure 7). One unique finding was that, even under low-O$_3$ conditions, negative
180 correlation was found between IO and O$_3$ concentrations in the daily dataset (Figures 3 and 7). Laboratory studies indicate that high O$_3$ concentrations can cause emission of iodine from ocean to atmosphere (Carpenter et al., 2013; Macdonald et al., 2014; Sakamoto et al., 2009). This "O$_3$-dependent" iodine release has been regarded as being more dominant than other "O$_3$-independent" types of emission, including photo-labile iodocarbons such as CH$_2$I$_2$, CH$_2$ICl, and their subsequent photolysis over the open oceans in every global-scale chemistry transport model representing iodine chemistry (Saiz-Lopez et al., 2014;
185 Sekiya et al., 2020; Sherwen et al., 2016). However, with an "O$_3$-dependent" HOI/I$_2$ flux of approximately 9×10^7 molecules cm^{-2} s^{-1} (section 2.2), as expected under an O$_3$ mixing ratio of approximately 10 ppbv, a zero-dimensional box model was not able to reproduce the negative correlation found between IO and O$_3$. Because the initial HOI/I$_2$ release flux limited by O$_3$ in the <12 ppbv mixing-ratio range cannot drive the strong O$_3$ reduction, the scenario produced only a positive correlation (Case 1, Figure 3). In contrast, another case in which the "O$_3$-independent" flux was added to compensate for the "O$_3$-dependent"
190 term weakened by a factor of 2 (Case 2, Figure 3) better reproduced the observed trend. The weakened flux might be explained by dissolved organic carbon (Shaw and Carpenter, 2013) or the presence of a sea-surface microlayer (Tinel et al., 2020) impeding iodine vaporization. The added "O$_3$-independent" flux is not explainable solely by flux from photolyses of

iodocarbons within the marine boundary layer (approximately 10^7 molecules cm^{-2} s^{-1}) generally assumed in the three-dimensional models (Saiz-Lopez et al., 2014; Sekiya et al., 2020; Sherwen et al., 2016). While indirectly considering the global total fluxes of CH_2IX (X = I, Br, Cl) as described by Ordóñez et al. (2012) in these model simulations, the "Chl-a-based" parameterization reduced the fluxes to too-low levels over this oceanic region. It therefore necessitates a survey of missing sources. The third case, with only an "O_3-independent" flux (Case 3, Figure 3) might explain the negative correlation more easily, whereas the total change of the flux type not being simply supported. We therefore hypothesize that O_3-independent processes are more important than has been represented by recent models. Indeed, a larger magnitude of organic iodine flux (approximately 7×10^7 molecules cm^{-2} s^{-1}) was reported in the low-latitude Pacific (Großmann et al., 2013), and would therefore be the most likely cause of the negative correlation. However, that study (Großmann et al., 2013) relied on assumption of an even larger inorganic iodine emission flux to explain the observed IO concentrations. Therefore, our analysis is the first to suggest that the "O_3-independent" flux can be comparably important to the "O_3-dependent" flux in this region. Other O_3-independent iodine release mechanisms such as photooxidation of aqueous I^- (Watanabe et al., 2019) might also be worth exploring. The modelled net O_3 loss rate attributable to iodine in Case 2 increased by up to 100% over that without iodine. The O_3 loss rate in the iodine cycle in Case 2 increased by approximately 15% over that in Case 1 (Table 4).

The expectation that a positive correlation between O_3 and IO would occur with O_3-dependent processes over a low O_3 concentration range was also confirmed using three-dimensional global chemistry-transport models including halogen chemistry (Sekiya et al., 2020; Saiz-Lopez et al., 2014) over the tropical western Pacific (Figures S2, S3). An alternative explanation for the observed negative correlation would be the mixing of air masses with different degrees of iodine chemistry. If so, such negative correlation could appear in the chemistry-transport model results. However, this feature was not found. Therefore, we propose an "O_3-independent" flux. Over the Atlantic, the O_3 mixing ratio rarely reaches these low levels (10 ppbv or less). Therefore, such process analyses have not been undertaken there. Under the influence of "O_3-independent" sources, even lower O_3 concentrations would be attainable. Radiative forcing of O_3, as estimated recently with halogen chemistry (Sherwen et al., 2017; Iglesias-Suarez et al., 2020; Saiz-Lopez et al., 2012; Hossaini et al., 2015), might be influenced by the dependence of iodine flux on O_3 concentration, which might play a major role in estimating past and future concentrations of O_3.

The time series of meteorological parameters including wind speed and SST was also investigated, but clear correlation such as that shown by O_3 and IO was not observed, in the correlation with O_3 or IO concentrations on a timescale of a few days (Figure 6). An earlier study (Kanaya et al., 2019) investigating the diurnal variation of O_3 in this area based on a comparison of observational data and a chemical transport model indicated that an as-yet-unidentified O_3 loss might occur over the tropical western Pacific. Our results imply that iodine chemistry plays an important role in O_3 loss in the area of SST maxima, which is regarded as an entry point from the troposphere to stratosphere. Moreover, these results provide insights into the manner by which increasing SST associated with climate change might modify the marine atmospheric chemical balance, which warrants further investigation. Results of recent studies indicate a roughly threefold increase in iodine since the 1950s, with at least 50% attributed to anthropogenic O_3 (Cuevas et al., 2018; Legrand et al., 2018; Zhao et al., 2019). If half of the

inorganic flux were O_3-independent, as suggested by Case 2, then either some other cause should be sought, or the change in O_3-dependent fluxes to produce the observed change is even more dramatic than previously thought. Further investigation of these points is necessary.

4. Summary

In this study, shipboard multi-axis differential optical absorption spectroscopy (MAX–DOAS), a remote sensing technique, was used during seven research cruises covering the widest latitudinal bands from the Arctic to the Southern Hemisphere as ever made with a single instrument, spanning SSTs of approximately 0°C to 31.5°C, allowing investigation of the variation of IO concentrations. It was particularly abundant over the tropical western Pacific (warm pool), appearing as an "iodine fountain", where SST maxima (>30°C) and O_3 minima are observed.

This report describes negative correlation between IO and O_3 concentrations over the IO maximum, even under extremely low O_3 conditions, which few earlier studies have demonstrated. This correlation is not explained easily by the O_3-dependent oceanic fluxes of photolabile inorganic iodine compounds adopted for recent simulation studies. Our findings rather imply that "O_3-independent" pathways which release iodine compounds from the ocean are also important. Iodine input to the atmosphere from the ocean surface is greater in areas of higher SST, leading to an "iodine fountain" in the Western Pacific warm pool because the I^- concentration in the ocean surface is likely to be higher in these areas. This higher concentration might contribute to more pronounced O_3 destruction over the Western Pacific warm pool than estimated earlier. Warming SSTs associated with climate change can change the atmospheric chemical balance through halogen chemistry, warranting further quantitative investigation.

Table 1: Cross-sections of iodine monoxide (IO) and O_4 differential slant column densities used for this study

	Component	Reference
	NO_2	Vandaele et al. (1998)
IO	O_3	Bogumil et al. (2000)
	H_2O	HITEMP* (Rothman et al., 2013)
	IO	Gómez-Martín et al. (2005)
	NO_2	Vandaele et al. (1998)
O_4	O_3	Bogumil et al. (2000)
	H_2O	HITEMP (Rothman et al., 2013)
	O_4	Thalman and Volkamer (2013)

* Correction factors from Lampel et al. (2015) were applied.

230

Table 2: Reactions of iodine chemistry added to RACM

Reactants	Products	A (cm^3 molecule^{-1} s^{-1})	Ea/R (K)	Reference
I + O$_3$	IO + O$_2$	2.10×10^{-11}	830	Sherwen et al. (2016)
I + HO$_2$	HI + O$_2$	1.50×10^{-11}	1090	Sherwen et al. (2016)
IO + NO	I + NO$_2$	7.15×10^{-12}	−300	Sherwen et al. (2016)
IO + HO$_2$	HOI + O$_2$	1.40×10^{-11}	−540	Sherwen et al. (2016)
IO + IO	0.43OIO + 0.71I + 0.43I$_2$O$_2$	9.60×10^{-11}	0	Stutz et al. (1999)
OH + HI	I + H$_2$O	1.60×10^{-11}	−440	Sherwen et al. (2016)
HOI + OH	IO + H$_2$O	5.00×10^{-12}	0	Sherwen et al. (2016)
I + NO$_3$	IO + NO$_2$	4.50×10^{-10}	0	Mcfiggans et al. (2000)
IO + CH$_3$O$_2$	0.25I + 0.254HCHO + 0.25HO$_2$ + 0.75HOI + 0.746ORA1 + 0.004H$_2$O$_2$	1.00×10^{-11}	0	Stutz et al. (1999)
IO + $h\nu$	I + O$_3$			Kanaya et al. (2007b)
HOI + $h\nu$	I + OH			Kanaya et al. (2007b)
INO$_2$ + $h\nu$	0.5I + 0.5NO$_2$ + 0.5IO + 0.5NO			Kanaya et al. (2007b)
IONO$_2$ + $h\nu$	0.5IO + 0.5NO$_2$ + 0.5I + 0.5NO$_3$			Kanaya et al. (2007b)
OIO + OH	HOI + O$_2$	7.00×10^{-12}	0	Kanaya et al. (2007b)
I$_2$O$_2$ + $h\nu$	I + OIO			Kanaya et al. (2007b)
I + NO$_2$ (+M)	INO$_2$ (+ M)	5.40×10^{-12}	0	Kanaya et al. (2003)
INO$_2$	I + NO$_2$	$9.94 \times 10^{+17}$	11859	Sherwen et al. (2016)
IO + NO$_2$ (+M)	IONO$_2$ (+ M)	3.70×10^{-12}	0	Kanaya et al. (2003)
IONO$_2$	IO + NO$_2$	$2.10 \times 10^{+15}$	13670	Sherwen et al. (2016)
I + NO (+M)	INO (+ M)	4.10×10^{-13}	0	Kanaya et al. (2003)
INO	I + NO	1.40×10^{-1}	0	Kanaya et al. (2003)
OIO + NO	IO + NO$_2$	1.10×10^{-12}	−542	Sherwen et al. (2016)
IO + ISOP	0.25I + 0.132MACR + 0.855OLT + 0.25HO$_2$ + 0.179HCHO + 0.75HOI + 0.075H$_2$O$_2$ + 0.9OH	1.00×10^{-11}	0	Kanaya et al. (2007b)
IBr + $h\nu$	I			Kanaya et al. (2007b)
OIO + $h\nu$	I + O$_2$			Kanaya et al. (2007c)
I$_2$ + OH	HOI + I	2.10×10^{-10}		Sherwen et al. (2016)
I$_2$ + NO$_3$	I + IONO$_2$	1.50×10^{-12}		Sherwen et al. (2016)
I$_2$ + $h\nu$	2I			Alicke et al. (1999)
IO + OIO	I$_2$O$_3$	1.5×10^{-10}		Sherwen et al. (2016)
OIO + OIO	I$_2$O$_4$	1.5×10^{-10}		Sherwen et al. (2016)
I$_2$O$_2$	OIO + I	1.13		Saiz-Lopez et al. (2016)
I$_2$O$_2$	IO + IO	0.00532		Saiz-Lopez et al. (2016)

I_2O_4	OIO + OIO	0.0879		Saiz-Lopez et al. (2016)
HOI + NO_3	IO + HNO_3	$2.7 \times 10^{-12} \times (300/T)^{2.66}$		Saiz-Lopez et al. (2016)
$I_2O_3 + hv$	IO + OIO			Saiz-Lopez et al. (2016)
$I_2O_4 + hv$	OIO + OIO			Saiz-Lopez et al. (2016)

235

Table 3: Research cruises of the R/V *Mirai* that generated data used for this study

Cruise	Period	Area
MR14-06 (leg 1)	8 Nov – 3 Dec, 2014	Western Pacific, Tropics
MR15-04	6 Nov – 21 Nov, 2015	Western Pacific, East Indian Ocean
MR15-05 (leg 2)	14 Jan – 24 Jan, 2016	Western Pacific
MR16-06	24 Aug – 4 Oct, 2016	Arctic Ocean, Bering Sea, North Pacific
MR16-09 (leg 3)	8 Feb – 3 Mar, 2017	Southern Ocean
MR17-05C	25 Aug – 29 Sep, 2017	Arctic Ocean, Bering Sea, North Pacific
MR17-08	22 Nov, 2017 – 17 Jan 2018	Western Pacific, East Indian Ocean

Table 4. Net and process-specific O_3 loss rates in three cases at an O_3 concentration of 10 ppbv, as calculated using the box model

	IO [ppbv]	net loss [ppbv d^{-1}]	HOx/Ox cycle loss [ppbv d^{-1}]	Iodine cycle loss [ppbv d^{-1}]
w.o. iodine	0	−1.06	−1.64	0
Case 1	0.553–0.741	−1.85 – −2.08	−1.62	−0.519 – −0.720
Case 2	0.611–0.851	−1.92 – −2.21	−1.62	−0.579 – −0.844
Case 3	0.723–0.960	−2.05 – −2.34	−1.62	−0.700 – −0.967

240
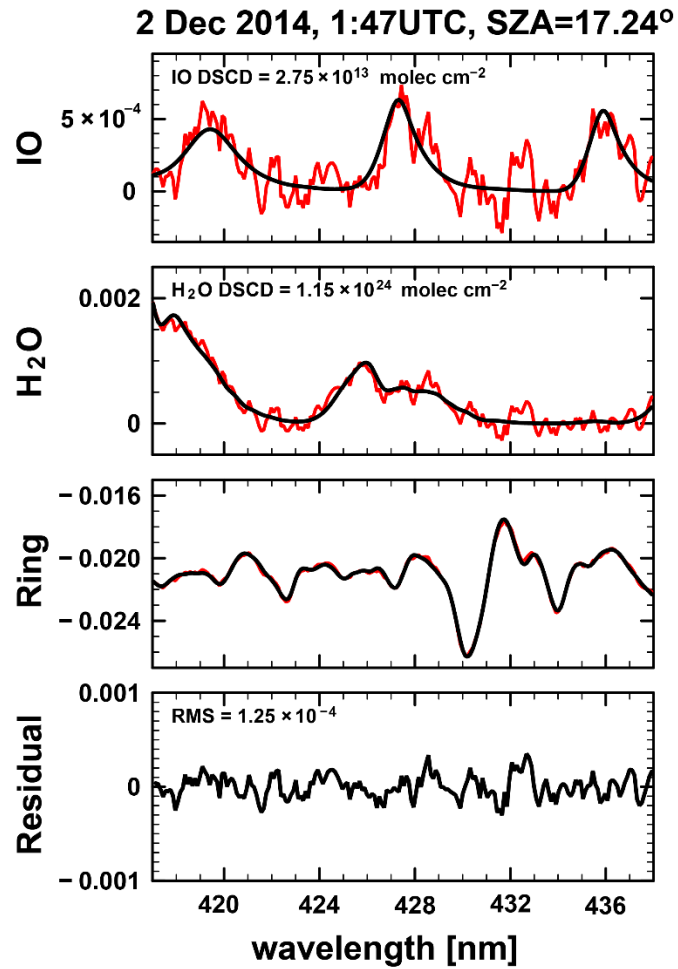
Figure 1: Nonlinear least-squares spectral fitting results for IO concentrations observed on 2 December 2014. The top two panels show fitting for IO and H2O. Black lines represent the cross-section scaled to the spectrum (red) determined by differential optical absorption spectroscopy. The lower two panels show the Ring-effect contribution and the residual spectrum.
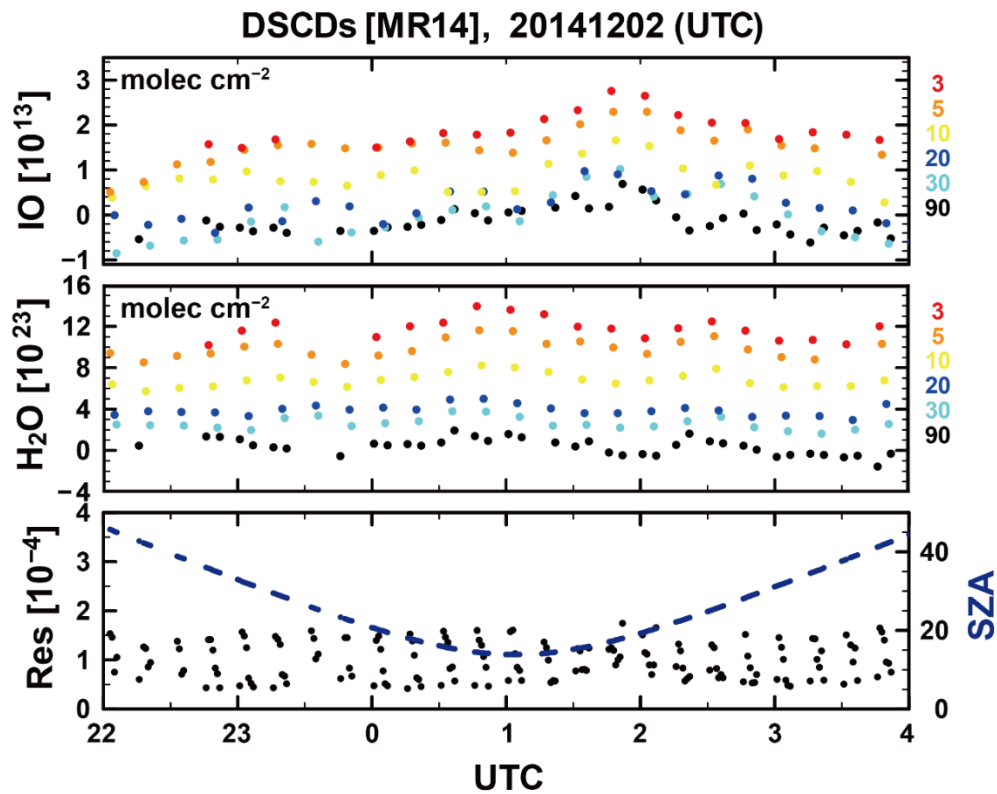
Figure 2: Time series of IO and H_2O differential slant column densities (DSCDs) for elevation angles of 3°, 5°, 10°, 20°, 30°, and 90°; RMS residual; and the solar zenith angle observed on 1–2 December 2014 over the tropical western Pacific.

245
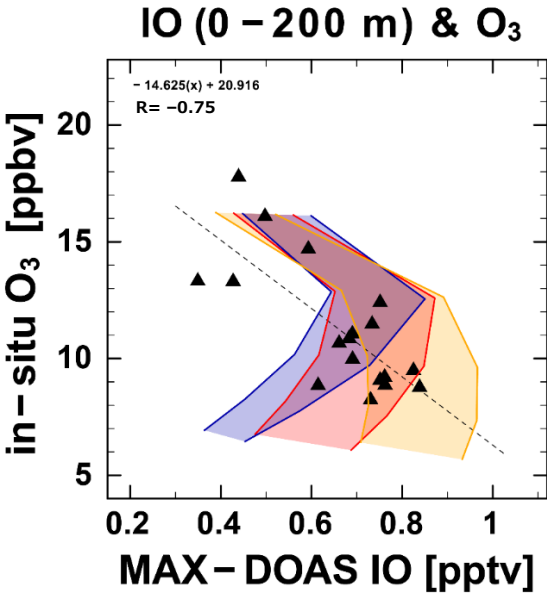
Figure 3: Daily median IO mixing ratio for 0–200 m (pptv) observed by MAX–DOAS versus daily median *in situ* ozone mixing ratio (ppbv). Results of box-model simulations with "O_3-dependent" (Case 1), "quasi-O_3-dependent" (Case 2), and "pure O_3 independent" (Case 3) emission fluxes of iodine compounds are superimposed respectively as blue-, red-, and orange-shaded areas.

250
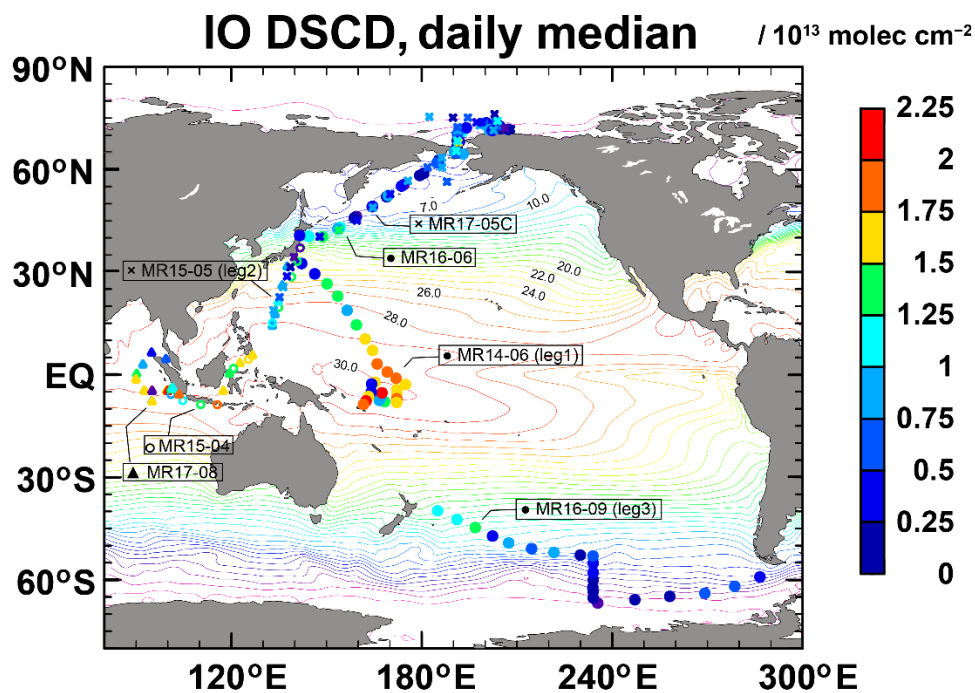
Figure 4: Daily median IO content (differential slant column densities (DSCD) for an elevation angle of 3°; molecules cm^{-2}) observed from the R/V *Mirai* during 2014–2018. Color contours represent the optimum interpolated SST averaged for 2014–2018.

255
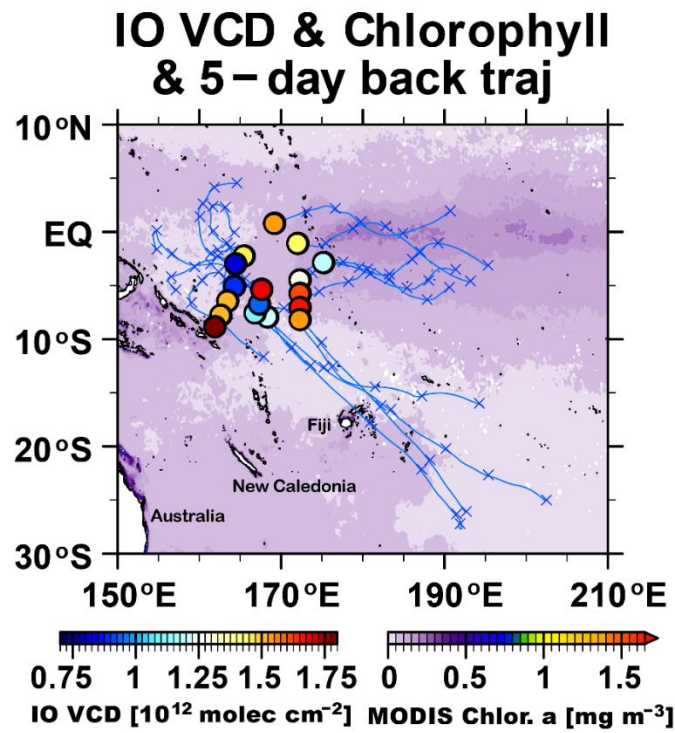
Figure 5: Daily median tropospheric IO vertical column densities (VCDs, molecules cm^{-2}) observed from the R/V *Mirai* during 16 November to 2 December 2014 and chlorophyll-a concentrations observed via satellite (MODIS). Blue crosses and lines represent five-day backward trajectories.
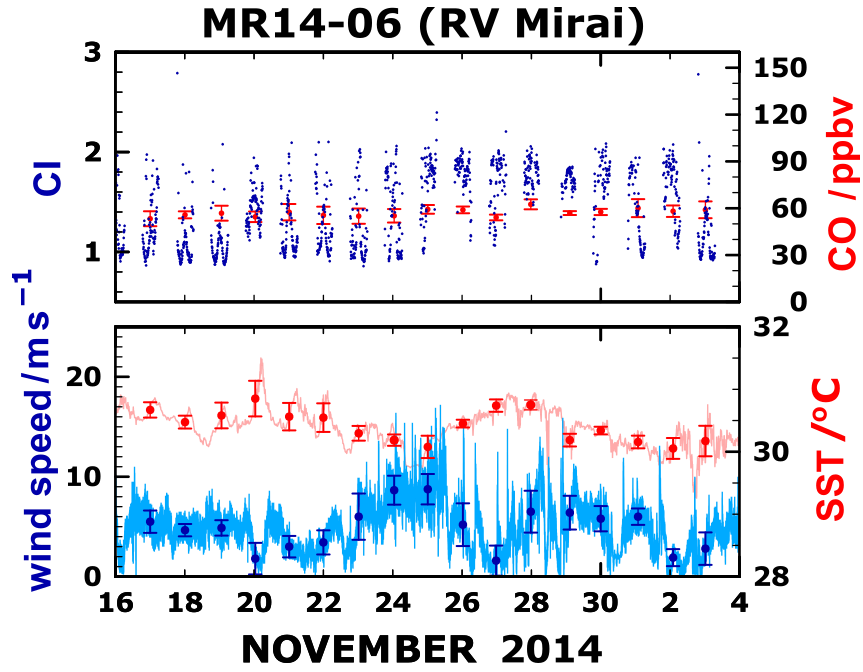
Figure 6: Time series of the CO mixing ratio [ppbv], color index (CI; defined as the ratio of the measured intensities at the two wavelengths of 500 and 380 nm (Takashima et al., 2009)), wind speed (m s^{-1}), and SST (°C).

260
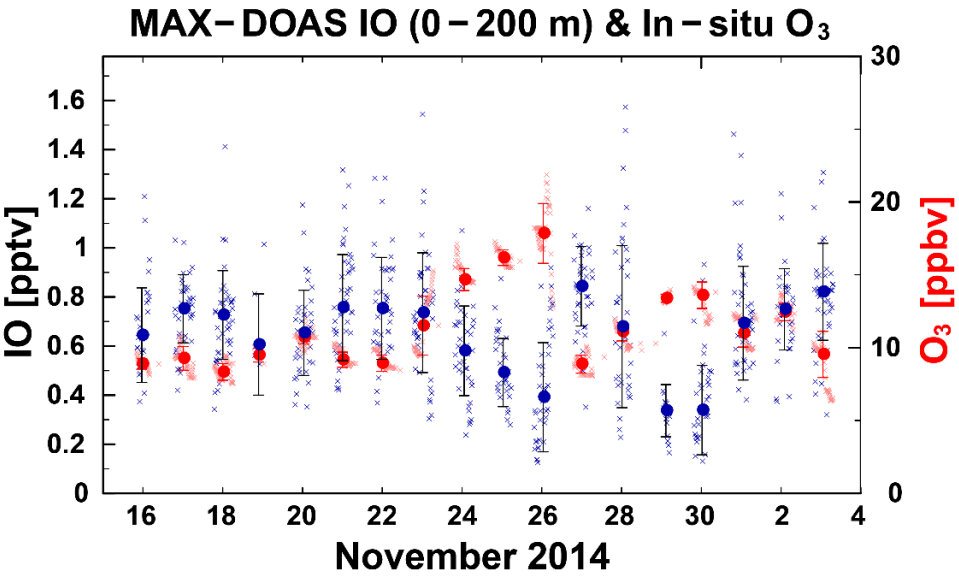
Figure 7: Time series of IO mixing ratio for 0–200 m (blue, pptv) observed by MAX–DOAS, and *in situ* O₃ mixing ratio (red, ppbv). Circles and horizontal bars respectively represent the daily median and one standard deviation.

Author contributions

HT designed the study, conducted shipboard MAX–DOAS observations and analyses, and wrote the manuscript. YKa proposed the research concept, supported the MAX–DOAS observations, and conducted O_3/CO observations and 0-D box model calculations. KS supported the observations and analysis. MF conducted the retrieval of IO profiles and IO VCDs. MV supported the DOAS analysis. FT, TM, and YKo supported the MAX–DOAS observations. CAC, AS-L, and TS conducted a simulation using a global chemical model. All co-authors provided comments to improve the manuscript.

Data availability

MAX-DOAS data are available by contacting the corresponding authors. Other data is available at the following sites (DARWIN).

MR14-06 (leg 1): https://doi.org/10.17596/0001862

MR15-04: https://doi.org/10.17596/0001975

MR15-05 (leg 2): https://doi.org/10.17596/0002030

MR16-06: https://doi.org/10.17596/0001870

MR16-09 (leg 3): https://doi.org/10.17596/0000026

MR17-05C: https://doi.org/10.17596/0001879

MR17-08 (leg1): https://doi.org/10.17596/0001881

MR17-08 (leg2): https://doi.org/10.17596/0001882

Supplement

Supporting information accompanies this paper.

Acknowledgments

We thank K. Kruger, Y. Yamashita, and K. Hara for their useful comments. We also thank Robert Spurr for free use of the VLIDORT radiative transfer code package. DOAS analysis involved the QDOAS software. We used MODIS chlorophyll *a*, OI SST, and ECMWF meteorological data. Figures were produced using the GFD-Dennou Library. This work was supported in part by funding from Fukuoka University (Grant No. 197103). This study has also received funding from the European Research Council Executive Agency under the European Union's Horizon 2020 Research and Innovation programme (Project 'ERC-2016-COG 726349 CLIMAHAL').

References

Alicke, B., Hebestreit, K., Stutz, J., and Platt, U.: Iodine oxide in the marine boundary layer, Nature, 397, 572-573, Doi 10.1038/17508, 1999.

295   Baccarini, A., Karlsson, L., Dommen, J., Duplessis, P., Vullers, J., Brooks, I. M., Saiz-Lopez, A., Salter, M., Tjernstrom, M., Baltensperger, U., Zieger, P., and Schmale, J.: Frequent new particle formation over the high Arctic pack ice by enhanced iodine emissions, Nat Commun, 11, 10.1038/s41467-020-18551-0, 2020.

Bogumil, K., Orphal, J., and Burrows, J. P.: Temperature-dependent absorption cross-sections of O_3, NO_2, and other atmospheric trace gases measured using the SCIAMACHY spectrometer, Proceedings of the ERS-Envisat Symposium,

300   2000.

Carpenter, L. J., Archer, S. D., and Beale, R.: Ocean-atmosphere trace gas exchange, Chem Soc Rev, 41, 6473-6506, 10.1039/c2cs35121h, 2012.

Carpenter, L. J., MacDonald, S. M., Shaw, M. D., Kumar, R., Saunders, R. W., Parthipan, R., Wilson, J., and Plane, J. M. C.: Atmospheric iodine levels influenced by sea surface emissions of inorganic iodine, Nat Geosci, 6, 108-111,

305   10.1038/Ngeo1687, 2013.

Chance, R., Baker, A. R., Carpenter, L., and Jickells, T. D.: The distribution of iodide at the sea surface, Environ Sci-Proc Imp, 16, 1841-1859, 10.1039/c4em00139g, 2014.

Chance, R. J., Tinel, L., Sherwen, T., Baker, A. R., Bell, T., Brindle, J., Campos, M., Croot, P., Ducklow, H., Peng, H., Hopkins, F., Hoogakker, B., Hughes, C., Jickells, T. D., Loades, D., Macaya, D. A. R., Mahajan, A. S., Malin, G., Phillips, D.,

310   Roberts, I., Roy, R., Sarkar, A., Sinha, A. K., Song, X., Winkelbauer, H., Wuttig, K., Yang, M., Peng, Z., and Carpenter, L. J.: Global sea-surface iodide observations, 1967-2018, Sci Data, 6, 286, 10.1038/s41597-019-0288-y, 2019.

Cuevas, C. A., Maffezzoli, N., Corella, J. P., Spolaor, A., Vallelonga, P., Kjaer, H. A., Simonsen, M., Winstrup, M., Vinther, B., Horvat, C., Fernandez, R. P., Kinnison, D., Lamarque, J. F., Barbante, C., and Saiz-Lopez, A.: Rapid increase in atmospheric iodine levels in the North Atlantic since the mid-20th century, Nat Commun, 9, 10.1038/s41467-018-03756-

315   1, 2018.

Danckaert, T., Fayt, C., Van Roozendael, M., De Smedt, I., Letocart, V., Merlaud, A., and Pinardi, G.: QDOAS software user manual, Belgian Institute for Space Aeronomy2017.

Davis, D., Crawford, J., Liu, S., McKeen, S., Bandy, A., Thornton, D., Rowland, F., and Blake, D.: Potential impact of iodine on tropospheric levels of ozone and other critical oxidants, J Geophys Res-Atmos, 101, 2135-2147, Doi

320   10.1029/95jd02727, 1996.

Dix, B., Baidara, S., Bresch, J. F., Hall, S. R., Schmidt, K. S., Wang, S. Y., and Volkamer, R.: Detection of iodine monoxide in the tropical free troposphere, P Natl Acad Sci USA, 110, 2035-2040, 10.1073/pnas.1212386110, 2013.

Friedrich, M. M., Rivera, C., Stremme, W., Ojeda, Z., Arellano, J., Bezanilla, A., Garcia-Reynoso, J. A., and Grutter, M.: NO$_2$ vertical profiles and column densities from MAX-DOAS measurements in Mexico City, Atmos Meas Tech, 12, 2545-2565, 10.5194/amt-12-2545-2019, 2019.

Frieß, U., Monks, P. S., Remedios, J. J., Rozanov, A., Sinreich, R., Wagner, T., and Platt, U.: MAX-DOAS O$_4$ measurements: A new technique to derive information on atmospheric aerosols: 2. Modeling studies, Journal of Geophysical Research, 111, 10.1029/2005jd006618, 2006.

Frieß, U., Beirle, S., Bonilla, L. A., Bosch, T., Friedrich, M. M., Hendrick, F., Piters, A., Richter, A., van Roozendael, M., Rozanov, V. V., Spinei, E., Tirpitz, J. L., Vlemmix, T., Wagner, T., and Wang, Y.: Intercomparison of MAX-DOAS vertical profile retrieval algorithms: studies using synthetic data, Atmos Meas Tech, 12, 2155-2181, 10.5194/amt-12-2155-2019, 2019.

Gómez-Martín, J. C., Spietz, P., and Burrows, J. P.: Spectroscopic studies of the I-2/O-3 photochemistry - Part 1: Determination of the absolute absorption cross sections of iodine oxides of atmospheric relevance, J Photoch Photobio A, 176, 15-38, 10.1016/j.jphotochem.2005.09.024, 2005.

Gómez-Martín, J. C., Lewis, T. R., Blitz, M. A., Plane, J. M. C., Kumar, M., Francisco, J. S., and Saiz-Lopez, A.: A gas-to-particle conversion mechanism helps to explain atmospheric particle formation through clustering of iodine oxides, Nat Commun, 11, 4521, 10.1038/s41467-020-18252-8, 2020.

Gómez-Martín, J. C., Saiz-Lopez, A., Cuevas, C. A., Fernandez, R. P., Gilfedder, B. S., Weller, R., Baker, A. R., Droste, E., and Lai, S.: Spatial and temporal variability of iodine in aerosol, J Geophys Res-Atmos, 126, 10.1002/essoar.10505416.1, 2021.

Gómez-Martín, J. C., Mahajan, A. S., Hay, T. D., Prados-Román, C., Ordóñez, C., MacDonald, S. M., Plane, J. M., Sorribas, M., Gil, M., and Paredes Mora, J. F.: Iodine chemistry in the eastern Pacific marine boundary layer, Journal of Geophysical Research: Atmospheres, 118, 887-904, 2013.

Großmann, K., Frieß, U., Peters, E., Wittrock, F., Lampel, J., Yilmaz, S., Tschritter, J., Sommariva, R., von Glasow, R., Quack, B., Krüger, K., Pfeilsticker, K., and Platt, U.: Iodine monoxide in the Western Pacific marine boundary layer, Atmos Chem Phys, 13, 3363-3378, 10.5194/acp-13-3363-2013, 2013.

Hayase, S., Yabushita, A., Kawasaki, M., Enami, S., Hoffmann, M. R., and Colussi, A. J.: Heterogeneous Reaction of Gaseous Ozone with Aqueous Iodide in the Presence of Aqueous Organic Species, J Phys Chem A, 114, 6016-6021, 10.1021/jp101985f, 2010.

Hayase, S., Yabushita, A., and Kawasaki, M.: Iodine Emission in the Presence of Humic Substances at the Water's Surface, J Phys Chem A, 116, 5779-5783, 10.1021/jp2048234, 2012.

He, X. C., Tham, Y. J., Dada, L., Wang, M. Y., Finkenzeller, H., Stolzenburg, D., Iyer, S., Simon, M., Kurten, A., Shen, J. L., Rorup, B., Rissanen, M., Schobesberger, S., Baalbaki, R., Wang, D. S., Koenig, T. K., Jokinen, T., Sarnela, N., Beck, L. J., Almeida, J., Amanatidis, S., Amorim, A., Ataei, F., Baccarini, A., Bertozzi, B., Bianchi, F., Brilke, S., Caudillo, L., Chen, D. X., Chiu, R., Chu, B. W., Dias, A., Ding, A. J., Dommen, J., Duplissy, J., El Haddad, I., Carracedo, L. G.,

Granzin, M., Hansel, A., Heinritzi, M., Hofbauer, V., Junninen, H., Kangasluoma, J., Kemppainen, D., Kim, C., Kong, W. M., Krechmer, J. E., Kvashin, A., Laitinen, T., Lamkaddam, H., Lee, C. P., Lehtipalo, K., Leiminger, M., Li, Z. J., Makhmutov, V., Manninen, H. E., Marie, G., Marten, R., Mathot, S., Mauldin, R. L., Mentler, B., Mohler, O., Muller, T., Nie, W., Onnela, A., Petaja, T., Pfeifer, J., Philippov, M., Ranjithkumar, A., Saiz-Lopez, A., Salma, I., Scholz, W., Schuchmann, S., Schulze, B., Steiner, G., Stozhkov, Y., Tauber, C., Tome, A., Thakur, R. C., Vaisanen, O., Vazquez-Pufleau, M., Wagner, A. C., Wang, Y. H., Weber, S. K., Winkler, P. M., Wu, Y. S., Xiao, M., Yan, C., Ye, Q., Ylisirnio, A., Zauner-Wieczorek, M., Zha, Q. Z., Zhou, P. T., Flagan, R. C., Curtius, J., Baltensperger, U., Kulmala, M., Kerminen, V. M., Kurten, T., Donahue, N. M., Volkamer, R., Kirkby, J., Worsnop, D. R., and Sipila, M.: Role of iodine oxoacids in atmospheric aerosol nucleation, Science, 371, 589-+, 10.1126/science.abe0298, 2021.

Henyey, L. G. and Greenstein, J. L.: Diffuse radiation in the Galaxy, Astrophys J, 93, 70-83, 10.1086/144246, 1941.

Holton, J. R., Haynes, P. H., Mcintyre, M. E., Douglass, A. R., Rood, R. B., and Pfister, L.: Stratosphere-Troposphere Exchange, Rev Geophys, 33, 403-439, Doi 10.1029/95rg02097, 1995.

Hönninger, G., von Friedeburg, C., and Platt, U.: Multi axis differential optical absorption spectroscopy (MAX-DOAS), Atmos Chem Phys, 4, 231-254, DOI 10.5194/acp-4-231-2004, 2004.

Hossaini, R., Chipperfield, M. P., Montzka, S. A., Rap, A., Dhomse, S., and Feng, W.: Efficiency of short-lived halogens at influencing climate through depletion of stratospheric ozone, Nat Geosci, 8, 186-190, 10.1038/Ngeo2363, 2015.

Iglesias-Suarez, F., Badia, A., Fernandez, R. P., Cuevas, C. A., Kinnison, D. E., Tilmes, S., Lamarque, J. F., Long, M. C., Hossaini, R., and Saiz-Lopez, A.: Natural halogens buffer tropospheric ozone in a changing climate, Nat Clim Change, 10, 147-154, 10.1038/s41558-019-0675-6, 2020.

Inamdar, S., Tinel, L., Chance, R., Carpenter, L. J., Sabu, P., Chacko, R., Tripathy, S. C., Kerkar, A. U., Sinha, A. K., Bhaskar, P. V., Sarkar, A., Roy, R., Sherwen, T., Cuevas, C., Saiz-Lopez, A., Ram, K., and Mahajan, A. S.: Estimation of reactive inorganic iodine fluxes in the Indian and Southern Ocean marine boundary layer, Atmos Chem Phys, 20, 12093-12114, 10.5194/acp-20-12093-2020, 2020.

Jones, C. E., Hornsby, K. E., Sommariva, R., Dunk, R. M., Von Glasow, R., McFiggans, G., and Carpenter, L. J.: Quantifying the contribution of marine organic gases to atmospheric iodine, Geophys Res Lett, 37, 10.1029/2010gl043990, 2010.

Kanaya, Y., Kajii, Y., and Akimoto, H.: Solar actinic flux and photolysis frequency determinations by radiometers and a radiative transfer model at Rishiri Island: comparisons, cloud effects, and detection of an aerosol plume from Russian forest fires, Atmos Environ, 37, 2463-2475, 10.1016/S1352-2310(03)00183-3, 2003.

Kanaya, Y., Cao, R. Q., Akimoto, H., Fukuda, M., Komazaki, Y., Yokouchi, Y., Koike, M., Tanimoto, H., Takegawa, N., and Kondo, Y.: Urban photochemistry in central Tokyo: 1. Observed and modeled OH and HO_2 radical concentrations during the winter and summer of 2004, J Geophys Res-Atmos, 112, 10.1029/2007jd008670, 2007a.

Kanaya, Y., Tanimoto, H., Matsumoto, J., Furutani, H., Hashimoto, S., Komazaki, Y., Tanaka, S., Yokouchi, Y., Kato, S., Kajii, Y., and Akimoto, H.: Diurnal variations in H_2O_2, O_3, PAN, HNO_3 and aldehyde concentrations and NO/NO_2 ratios

390  at Rishiri Island, Japan: Potential influence from iodine chemistry, Sci Total Environ, 376, 185-197, 10.1016/j.scitotenv.2007.01.073, 2007b.

Kanaya, Y., Miyazaki, K., Taketani, F., Miyakawa, T., Takashima, H., Komazaki, Y., Pan, X. L., Kato, S., Sudo, K., Sekiya, T., Inoue, J., Sato, K., and Oshima, K.: Ozone and carbon monoxide observations over open oceans on R/V Mirai from 67 degrees S to 75 degrees N during 2012 to 2017: testing global chemical reanalysis in terms of Arctic processes, low

395  ozone levels at low latitudes, and pollution transport, Atmos Chem Phys, 19, 7233-7254, 10.5194/acp-19-7233-2019, 2019.

Kanaya, Y., Irie, H., Takashima, H., Iwabuchi, H., Akimoto, H., Sudo, K., Gu, M., Chong, J., Kim, Y. J., Lee, H., Li, A., Si, F., Xu, J., Xie, P. H., Liu, W. Q., Dzhola, A., Postylyakov, O., Ivanov, V., Grechko, E., Terpugova, S., and Panchenko, M.: Long-term MAX-DOAS network observations of NO$_2$ in Russia and Asia (MADRAS) during the period 2007-2012:

400  instrumentation, elucidation of climatology, and comparisons with OMI satellite observations and global model simulations, Atmos Chem Phys, 14, 7909-7927, 10.5194/acp-14-7909-2014, 2014.

Kanaya, Y. G., Cao, R. Q., Kato, S. G., Miyakawa, Y. K., Kajii, Y., Tanimoto, H., Yokouchi, Y., Mochida, M., Kawamura, K., and Akimoto, H.: Chemistry of OH and HO$_2$ radicals observed at Rishiri Island, Japan, in September 2003: Missing daytime sink of HO$_2$ and positive nighttime correlations with monoterpenes, J Geophys Res-Atmos, 112,

405  10.1029/2006jd007987, 2007c.

Kley, D., Crutzen, P. J., Smit, H. G. J., Vomel, H., Oltmans, S. J., Grassl, H., and Ramanathan, V.: Observations of near-zero ozone concentrations over the convective Pacific: Effects on air chemistry, Science, 274, 230-233, DOI 10.1126/science.274.5285.230, 1996.

Koenig, T. K., Baidar, S., Campuzano-Jost, P., Cuevas, C. A., Dix, B., Fernandez, R. P., Guo, H., Hall, S. R., Kinnison, D.,

410  Nault, B. A., Ullmann, K., Jimenez, J. L., Saiz-Lopez, A., and Volkamer, R.: Quantitative detection of iodine in the stratosphere, P Natl Acad Sci USA, 117, 1860-1866, 10.1073/pnas.1916828117, 2020.

Koenig, T. K., Volkamer, R., Baidar, S., Dix, B., Wang, S. Y., Anderson, D. C., Salawitch, R. J., Wales, P. A., Cuevas, C. A., Fernandez, R. P., Saiz-Lopez, A., Evans, M. J., Sherwen, T., Jacob, D. J., Schmidt, J., Kinnison, D., Lamarque, J. F., Apel, E. C., Bresch, J. C., Campos, T., Flocke, F. M., Hall, S. R., Honomichl, S. B., Hornbrook, R., Jensen, J. B., Lueb, R.,

415  Montzka, D. D., Pan, L. L., Reeves, J. M., Schauffler, S. M., Ullmann, K., Weinheimer, A. J., Atlas, E. L., Donets, V., Navarro, M. A., Riemer, D., Blake, N. J., Chen, D. X., Huey, L. G., Tanner, D. J., Hanisco, T. F., and Wolfe, G. M.: BrO and inferred Br-y profiles over the western Pacific: relevance of inorganic bromine sources and a Br-y minimum in the aged tropical tropopause layer, Atmos Chem Phys, 17, 15245-15270, 10.5194/acp-17-15245-2017, 2017.

Lampel, J., Frieß, U., and Platt, U.: The impact of vibrational Raman scattering of air on DOAS measurements of atmospheric

420  trace gases, Atmos Meas Tech, 8, 3767-3787, 10.5194/amt-8-3767-2015, 2015.

Legrand, M., McConnell, J. R., Preunkert, S., Arienzo, M., Chellman, N., Gleason, K., Sherwen, T., Evans, M. J., and Carpenter, L. J.: Alpine ice evidence of a three-fold increase in atmospheric iodine deposition since 1950 in Europe due to increasing oceanic emissions, P Natl Acad Sci USA, 115, 12136-12141, 10.1073/pnas.1809867115, 2018.

MacDonald, S. M., Martin, J. C. G., Chance, R., Warriner, S., Saiz-Lopez, A., Carpenter, L. J., and Plane, J. M. C.: A laboratory
425   characterisation of inorganic iodine emissions from the sea surface: dependence on oceanic variables and parameterisation
for global modelling, Atmos Chem Phys, 14, 5841-5852, 10.5194/acp-14-5841-2014, 2014.

Mahajan, A. S., Martin, J. C. G., Hay, T. D., Royer, S. J., Yvon-Lewis, S., Liu, Y., Hu, L., Prados-Roman, C., Ordonez, C.,
Plane, J. M. C., and Saiz-Lopez, A.: Latitudinal distribution of reactive iodine in the Eastern Pacific and its link to open
ocean sources, Atmos Chem Phys, 12, 11609-11617, 10.5194/acp-12-11609-2012, 2012.

430 McFiggans, G., Plane, J. M. C., Allan, B. J., Carpenter, L. J., Coe, H., and O'Dowd, C.: A modeling study of iodine chemistry
in the marine boundary layer, J Geophys Res-Atmos, 105, 14371-14385, Doi 10.1029/1999jd901187, 2000.

O'Dowd, C. D., Jimenez, J. L., Bahreini, R., Flagan, R. C., Seinfeld, J. H., Hameri, K., Pirjola, L., Kulmala, M., Jennings, S.
G., and Hoffmann, T.: Marine aerosol formation from biogenic iodine emissions, Nature, 417, 632-636, DOI
10.1038/nature00775, 2002.

435 Ordóñez, C., Lamarque, J. F., Tilmes, S., Kinnison, D. E., Atlas, E. L., Blake, D. R., Santos, G. S., Brasseur, G., and Saiz-
Lopez, A.: Bromine and iodine chemistry in a global chemistry-climate model: description and evaluation of very short-
lived oceanic sources, Atmos Chem Phys, 12, 1423-1447, 10.5194/acp-12-1423-2012, 2012.

Platt, U. and Stutz, J.: Differential Optical Absorption Spectroscopy, Physics of Earth and Space Environments, Springer-
Verlag Berlin Heidelberg, 10.1007/978-3-540-75776-4, 2008.

440 Pound, R. J., Sherwen, T., Helmig, D., Carpenter, L. J., and Evans, M. J.: Influences of oceanic ozone deposition on
tropospheric photochemistry, Atmos Chem Phys, 20, 4227-4239, 10.5194/acp-20-4227-2020, 2020.

Prados-Roman, C., Cuevas, C. A., Hay, T., Fernandez, R. P., Mahajan, A. S., Royer, S. J., Gali, M., Simo, R., Dachs, J.,
Großmann, K., Kinnison, D. E., Lamarque, J. F., and Saiz-Lopez, A.: Iodine oxide in the global marine boundary layer,
Atmos Chem Phys, 15, 583-593, 10.5194/acp-15-583-2015, 2015a.

445 Prados-Roman, C., Cuevas, C. A., Fernandez, R. P., Kinnison, D. E., Lamarque, J. F., and Saiz-Lopez, A.: A negative feedback
between anthropogenic ozone pollution and enhanced ocean emissions of iodine, Atmos Chem Phys, 15, 2215-2224,
10.5194/acp-15-2215-2015, 2015b.

Read, K. A., Mahajan, A. S., Carpenter, L. J., Evans, M. J., Faria, B. V. E., Heard, D. E., Hopkins, J. R., Lee, J. D., Moller, S.
J., Lewis, A. C., Mendes, L., McQuaid, J. B., Oetjen, H., Saiz-Lopez, A., Pilling, M. J., and Plane, J. M. C.: Extensive
450   halogen-mediated ozone destruction over the tropical Atlantic Ocean, Nature, 453, 1232-1235, 10.1038/nature07035,
2008.

Rex, M., Wohltmann, I., Ridder, T., Lehmann, R., Rosenlof, K., Wennberg, P., Weisenstein, D., Notholt, J., Kruger, K., Mohr,
V., and Tegtmeier, S.: A tropical West Pacific OH minimum and implications for stratospheric composition, Atmos Chem
Phys, 14, 4827-4841, 10.5194/acp-14-4827-2014, 2014.

455 Rothman, L. S., Gordon, I. E., Babikov, Y., Barbe, A., Benner, D. C., Bernath, P. F., Birk, M., Bizzocchi, L., Boudon, V.,
Brown, L. R., Campargue, A., Chance, K., Cohen, E. A., Coudert, L. H., Devi, V. M., Drouin, B. J., Fayt, A., Flaud, J.
M., Gamache, R. R., Harrison, J. J., Hartmann, J. M., Hill, C., Hodges, J. T., Jacquemart, D., Jolly, A., Lamouroux, J., Le

Roy, R. J., Li, G., Long, D. A., Lyulin, O. M., Mackie, C. J., Massie, S. T., Mikhailenko, S., Muller, H. S. P., Naumenko, O. V., Nikitin, A. V., Orphal, J., Perevalov, V., Perrin, A., Polovtseva, E. R., Richard, C., Smith, M. A. H., Starikova, E., Sung, K., Tashkun, S., Tennyson, J., Toon, G. C., Tyuterev, V. G., and Wagner, G.: The HITRAN2012 molecular spectroscopic database, J Quant Spectrosc Ra, 130, 4-50, 10.1016/j.jqsrt.2013.07.002, 2013.

Saiz-Lopez, A., Plane, J. M. C., Cuevas, C. A., Mahajan, A. S., Lamarque, J. F., and Kinnison, D. E.: Nighttime atmospheric chemistry of iodine, Atmos. Chem. Phys., 16, 15593-15604, 10.5194/acp-16-15593-2016, 2016.

Saiz-Lopez, A., Fernandez, R. P., Ordonez, C., Kinnison, D. E., Martin, J. C. G., Lamarque, J. F., and Tilmes, S.: Iodine chemistry in the troposphere and its effect on ozone, Atmos Chem Phys, 14, 13119-13143, 10.5194/acp-14-13119-2014, 2014.

Saiz-Lopez, A., Baidar, S., Cuevas, C. A., Koenig, T. K., Fernandez, R. P., Dix, B., Kinnison, D. E., Lamarque, J. F., Rodriguez-Lloveras, X., Campos, T. L., and Volkamer, R.: Injection of iodine to the stratosphere, Geophys Res Lett, 42, 6852-6859, 10.1002/2015gl064796, 2015.

Saiz-Lopez, A., Lamarque, J. F., Kinnison, D. E., Tilmes, S., Ordonez, C., Orlando, J. J., Conley, A. J., Plane, J. M. C., Mahajan, A. S., Santos, G. S., Atlas, E. L., Blake, D. R., Sander, S. P., Schauffler, S., Thompson, A. M., and Brasseur, G.: Estimating the climate significance of halogen-driven ozone loss in the tropical marine troposphere, Atmos Chem Phys, 12, 3939-3949, 10.5194/acp-12-3939-2012, 2012.

Sakamoto, Y., Yabushita, A., Kawasaki, M., and Enami, S.: Direct emission of I_2 molecule and IO radical from the heterogeneous reactions of gaseous ozone with aqueous potassium iodide solution, J Phys Chem A, 113, 7707-7713, 10.1021/jp903486u, 2009.

Sekiya, T., Kanaya, Y., Sudo, K., Taketani, F., Iwamoto, Y., Aita, M. N., Yamamoto, A., and Kawamoto, K.: Global Bromine- and Iodine-Mediated Tropospheric Ozone Loss Estimated Using the CHASER Chemical Transport Model, Sola, 16, 220-227, 10.2151/sola.2020-037, 2020.

Shaw, M. D. and Carpenter, L. J.: Modification of Ozone Deposition and I-2 Emissions at the Air-Aqueous Interface by Dissolved Organic Carbon of Marine Origin, Environ Sci Technol, 47, 10947-10954, 10.1021/es4011459, 2013.

Sherwen, T., Evans, M. J., Carpenter, L. J., Schmidt, J. A., and Mickley, L. J.: Halogen chemistry reduces tropospheric O-3 radiative forcing, Atmos Chem Phys, 17, 1557-1569, 10.5194/acp-17-1557-2017, 2017.

Sherwen, T., Schmidt, J. A., Evans, M. J., Carpenter, L. J., Großmann, K., Eastham, S. D., Jacob, D. J., Dix, B., Koenig, T. K., Sinreich, R., Ortega, I., Volkamer, R., Saiz-Lopez, A., Prados-Roman, C., Mahajan, A. S., and Ordonez, C.: Global impacts of tropospheric halogens (Cl, Br, I) on oxidants and composition in GEOS-Chem, Atmos Chem Phys, 16, 12239-12271, 10.5194/acp-16-12239-2016, 2016.

Simpson, W. R., Brown, S. S., Saiz-Lopez, A., Thornton, J. A., and von Glasow, R.: Tropospheric Halogen Chemistry: Sources, Cycling, and Impacts, Chem Rev, 115, 4035-4062, 10.1021/cr5006638, 2015.

Sinreich, R., Frieß, U., Wagner, T., and Platt, U.: Multi axis differential optical absorption spectroscopy (MAX-DOAS) of gas and aerosol distributions, Faraday Discuss, 130, 153-164; discussion 241-164, 519-124, 10.1039/b419274p, 2005.

Sipila, M., Sarnela, N., Jokinen, T., Henschel, H., Junninen, H., Kontkanen, J., Richters, S., Kangasluoma, J., Franchin, A., Perakyla, O., Rissanen, M. P., Ehn, M., Vehkamaki, H., Kurten, T., Berndt, T., Petaja, T., Worsnop, D., Ceburnis, D., Kerminen, V. M., Kulmala, M., and O'Dowd, C.: Molecular-scale evidence of aerosol particle formation via sequential addition of HIO_3, Nature, 537, 532-534, 10.1038/nature19314, 2016.

Spurr, R. J. D.: VLIDORT: A linearized pseudo-spherical vector discrete ordinate radiative transfer code for forward model and retrieval studies in multilayer multiple scattering media, J Quant Spectrosc Ra, 102, 316-342, 10.1016/j.jqsrt.2006.05.005, 2006.

Stockwell, W. R., Kirchner, F., Kuhn, M., and Seefeld, S.: A new mechanism for regional atmospheric chemistry modeling, J Geophys Res-Atmos, 102, 25847-25879, Doi 10.1029/97jd00849, 1997.

Stutz, J., Hebestreit, K., Alicke, B., and Platt, U.: Chemistry of halogen oxides in the troposphere: Comparison of model calculations with recent field data, J Atmos Chem, 34, 65-85, Doi 10.1023/A:1006245802825, 1999.

Takashima, H., Kanaya, Y., and Taketani, F.: Downsizing of a ship-borne MAX-DOAS instrument, JAMSTEC Report of Research and Development, 23, 34-40, 10.5918/jamstecr.23.34, 2016.

Takashima, H., Irie, H., Kanaya, Y., and Akimoto, H.: Enhanced NO_2 at Okinawa Island, Japan caused by rapid air-mass transport from China as observed by MAX-DOAS, Atmos Environ, 45, 2593-2597, 10.1016/j.atmosenv.2010.10.055, 2011.

Takashima, H., Irie, H., Kanaya, Y., and Syamsudin, F.: NO_2 observations over the western Pacific and Indian Ocean by MAX-DOAS on Kaiyo, a Japanese research vessel, Atmos Meas Tech, 5, 2351-2360, 10.5194/amt-5-2351-2012, 2012.

Takashima, H., Shiotani, M., Fujiwara, M., Nishi, N., and Hasebe, F.: Ozonesonde observations at Christmas Island (2 degrees N, 157 degrees W) in the equatorial central Pacific, J Geophys Res-Atmos, 113, 10.1029/2007jd009374, 2008.

Takashima, H., Irie, H., Kanaya, Y., Shimizu, A., Aoki, K., and Akimoto, H.: Atmospheric aerosol variations at Okinawa Island in Japan observed by MAX-DOAS using a new cloud-screening method, J Geophys Res-Atmos, 114, 10.1029/2009jd011939, 2009.

Thalman, R. and Volkamer, R.: Temperature dependent absorption cross-sections of O-2-O-2 collision pairs between 340 and 630 nm and at atmospherically relevant pressure, Phys Chem Chem Phys, 15, 15371-15381, 10.1039/c3cp50968k, 2013.

Tinel, L., Adams, T. J., Hollis, L. D. J., Bridger, A. J. M., Chance, R. J., Ward, M. W., Ball, S. M., and Carpenter, L. J.: Influence of the Sea Surface Microlayer on Oceanic Iodine Emissions, Environ Sci Technol, 54, 13228-13237, 10.1021/acs.est.0c02736, 2020.

Tirpitz, J. L., Frieß, U., Hendrick, F., Alberti, C., Allaart, M., Apituley, A., Bais, A., Beirle, S., Berkhout, S., Bognar, K., Bosch, T., Bruchkouski, I., Cede, A., Chan, K. L., den Hoed, M., Donner, S., Drosoglou, T., Fayt, C., Friedrich, M. M., Frumau, A., Gast, L., Gielen, C., Gomez-Martin, L., Hao, N., Hensen, A., Henzing, B., Hermans, C., Jin, J. L., Kreher, K., Kuhn, J., Lampel, J., Li, A., Liu, C., Liu, H. R., Ma, J. Z., Merlaud, A., Peters, E., Pinardi, G., Piters, A., Platt, U., Puentedura, O., Richter, A., Schmitt, S., Spinei, E., Zweers, D. S., Strong, K., Swart, D., Tack, F., Tiefengraber, M., van der Hoff, R., van Roozendael, M., Vlemmix, T., Vonk, J., Wagner, T., Wang, Y., Wang, Z. R., Wenig, M., Wiegner, M.,

Wittrock, F., Xie, P. H., Xing, C. Z., Xu, J., Yela, M., Zhang, C. X., and Zhao, X. Y.: Intercomparison of MAX-DOAS vertical profile retrieval algorithms: studies on field data from the CINDI-2 campaign, Atmos Meas Tech, 14, 1-35, 10.5194/amt-14-1-2021, 2021.

Tsunogai, S. and Henmi, T.: Iodine in the surface water of the ocean, Journal of the Oceanographical Society of Japan, 27, 67-72, 10.1007/BF02109332, 1971.

Vandaele, A. C., Hermans, C., Simon, P. C., Carleer, M., Colin, R., Fally, S., Merienne, M. F., Jenouvrier, A., and Coquart, B.: Measurements of the NO_2 absorption cross-section from 42 000 cm(-1) to 10 000 cm(-1) (238-1000 nm) at 220 K and 294 K, J Quant Spectrosc Ra, 59, 171-184, Doi 10.1016/S0022-4073(97)00168-4, 1998.

Volkamer, R., Coburn, S., Dix, B., and Sinreich, R.: MAX-DOAS observations from ground, ship, and research aircraft: maximizing signal-to-noise to measure 'weak' absorbers, Proc.SPIE, 7462, 10.1117/12.826792, 2009.

Volkamer, R., Baidar, S., Campos, T. L., Coburn, S., DiGangi, J. P., Dix, B., Eloranta, E. W., Koenig, T. K., Morley, B., Ortega, I., Pierce, B. R., Reeves, M., Sinreich, R., Wang, S., Zondlo, M. A., and Romashkin, P. A.: Aircraft measurements of BrO, IO, glyoxal, NO_2, H_2O, O_2-O_2 and aerosol extinction profiles in the tropics: comparison with aircraft-/ship-based in situ and lidar measurements, Atmos Meas Tech, 8, 2121-2148, 10.5194/amt-8-2121-2015, 2015.

Wagner, T., Dix, B., von Friedeburg, C., Frieß, U., Sanghavi, S., Sinreich, R., and Platt, U.: MAX-DOAS O-4 measurements: A new technique to derive information on atmospheric aerosols - Principles and information content, J Geophys Res-Atmos, 109, 10.1029/2004jd004904, 2004.

Watanabe, K., Matsuda, S., Cuevas, C. A., Saiz-Lopez, A., Yabushita, A., and Nakano, Y.: Experimental Determination of the Photooxidation of Aqueous I- as a Source of Atmospheric I-2, Acs Earth Space Chem, 3, 669-679, 10.1021/acsearthspacechem.9b00007, 2019.

Wittrock, F., Oetjen, H., Richter, A., Fietkau, S., Medeke, T., Rozanov, A., and Burrows, J. P.: MAX-DOAS measurements of atmospheric trace gases in Ny-Alesund - Radiative transfer studies and their application, Atmos Chem Phys, 4, 955-966, DOI 10.5194/acp-4-955-2004, 2004.

Zhao, X., Hou, X. L., and Zhou, W. J.: Atmospheric Iodine (I-127 and I-129) Record in Spruce Tree Rings in the Northeast Qinghai-Tibet Plateau, Environ Sci Technol, 53, 8706-8714, 10.1021/acs.est.9b01160, 2019.

Supplement

Figures S1 to S6.

555

Ozone mixing ratio observed from the R/V *Mirai* during seven research cruises during 2014–2018 are presented in Figure S1. Minimum concentrations of O_3 were observed over the tropical western Pacific. Correlation between O_3 and IO simulated by two global chemistry-transport models over the tropical western Pacific are shown in Figures S2 and S3. In the low ozone concentration range (e.g., <12 ppb), positive correlations between ozone and IO concentrations were evident for the two global

560 chemistry-transport models including halogen chemistry, where the "O_3-dependent" flux was dominant. Diurnal variations of IO mixing ratio for 0–200 m during MR14-06 (leg1) are shown in Figure S4. No clear diurnal variation is observed, but large day-to-day variation is observed. Scatter diagram between SST and IO DSCDs over the remote ocean are shown in Figure S5. High IO contents are observed over high SST region (> 30°C).

565
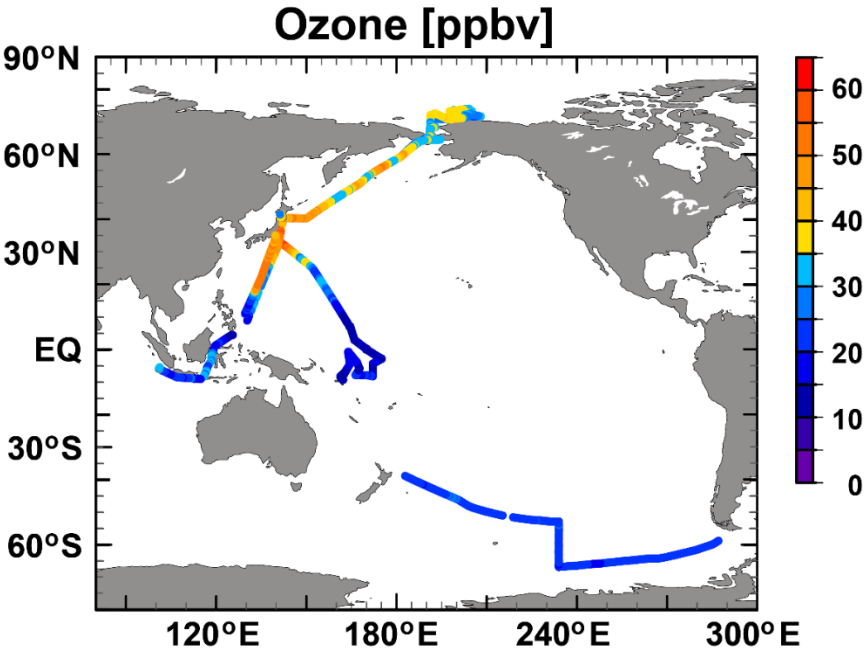
Figure S1: Ozone mixing ratio [ppbv] observed from the R/V *Mirai* cruises presented in Table 1 during 2014–2018.

570
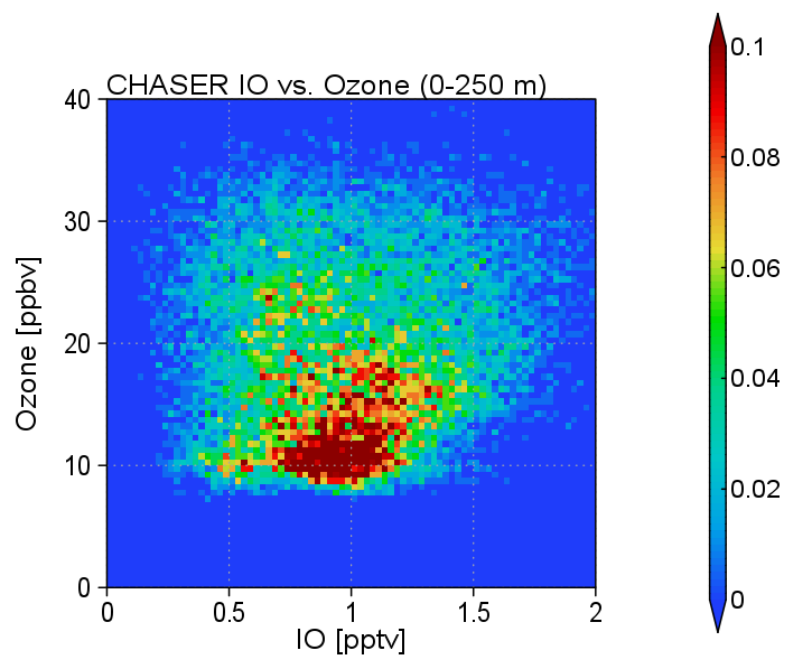
Figure S2: Two-dimensional histogram [%] as a function of IO volume mixing ratio [pptv] and ozone mixing ratio [ppbv] for 0–250 m altitudes simulated using a global chemical model (Sekiya et al., 2020) during the observation period (Nov–Dec 2014) over the tropical western Pacific (0–15°N, 150–165°E).
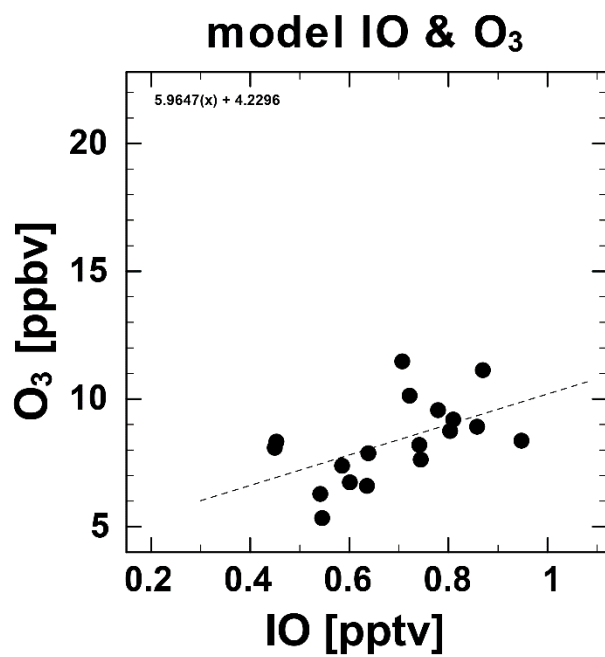
Figure S3: Scatterplot of IO mixing ratio [pptv] and ozone mixing ratio [ppbv] simulated by global chemical model (Saiz-Lopez et al., 2014) along the cruise track (MR14-06) over the tropical western Pacific.

585
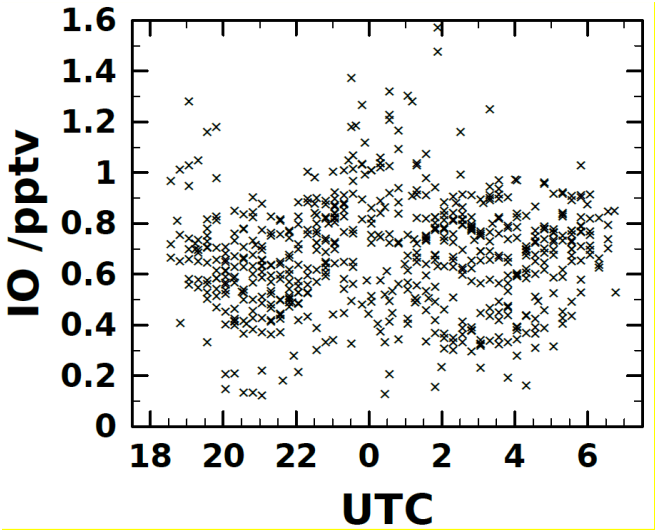
Figure S4: Diurnal variation of IO mixing ratio for 0–200 m [pptv] during the MR14-06 (leg1) cruise.

590
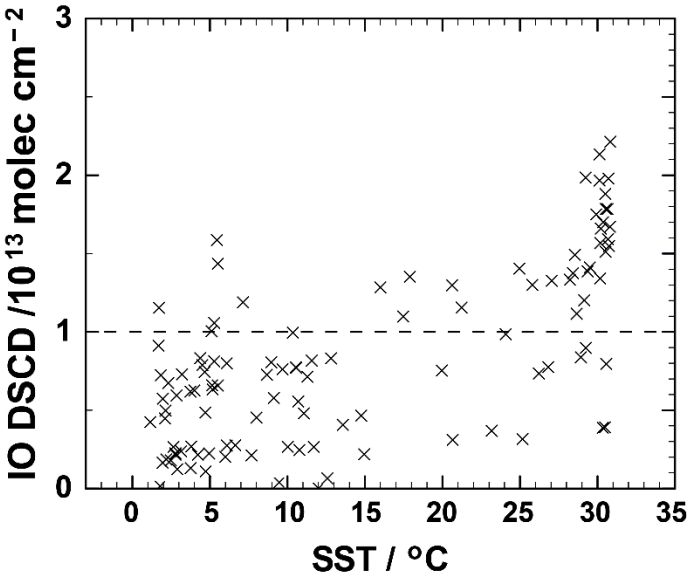
Figure S5: Scatter plot of SST [°C] and IO DSCD (el = 3°) [10^{13} molecules cm^{-2}] over the remote ocean.

595
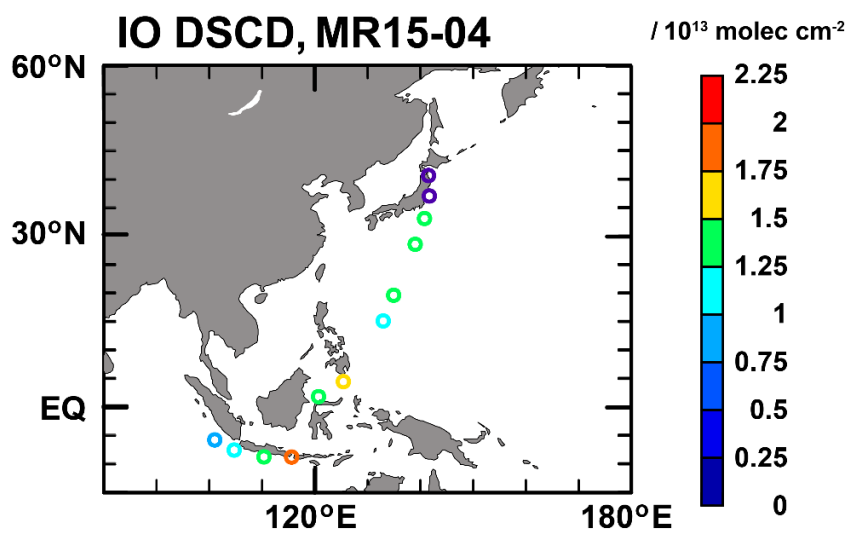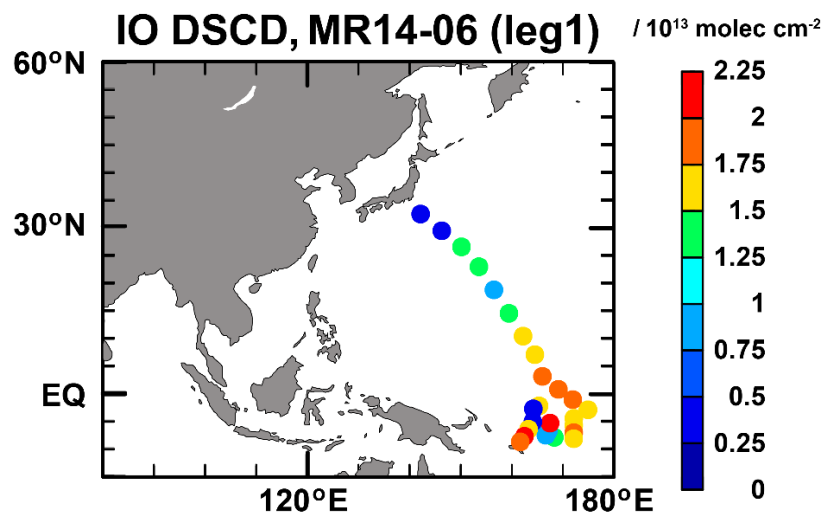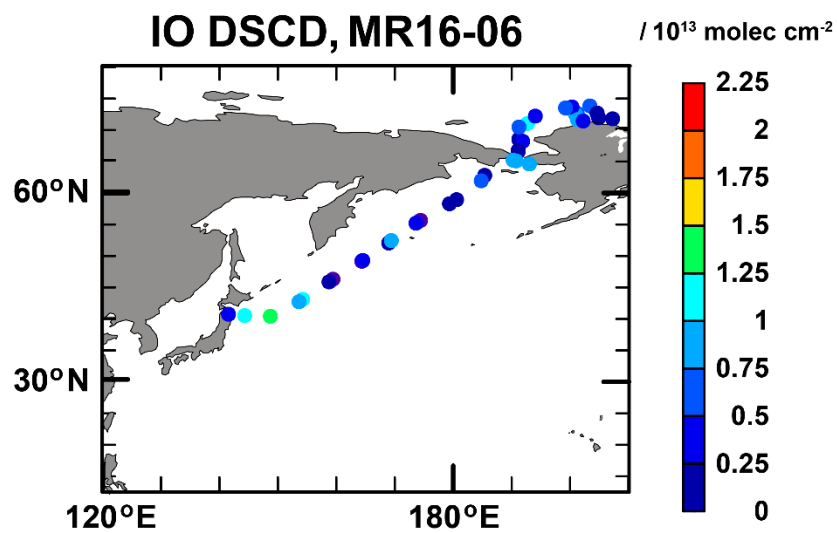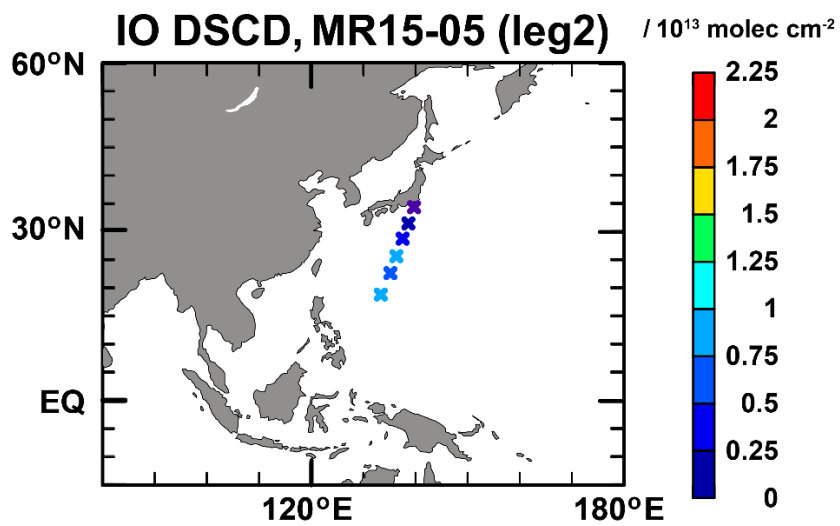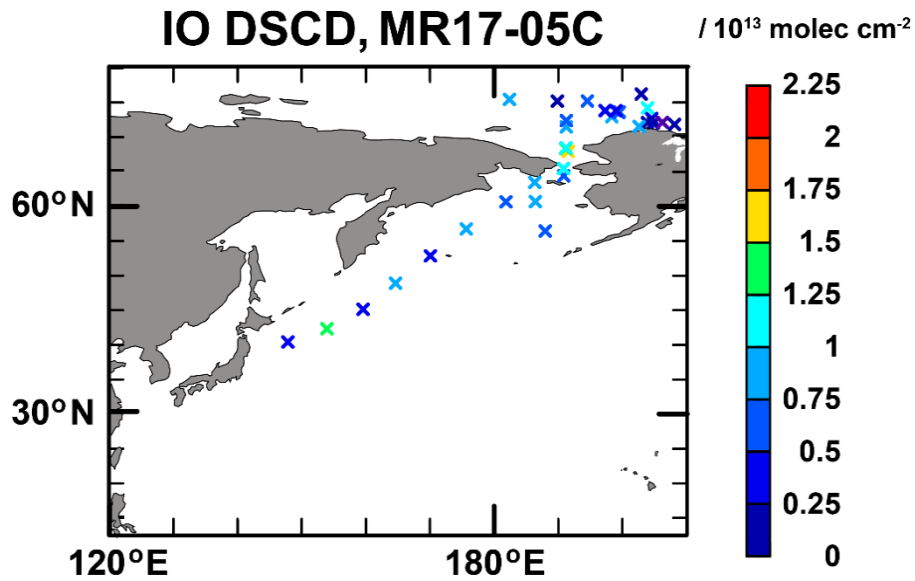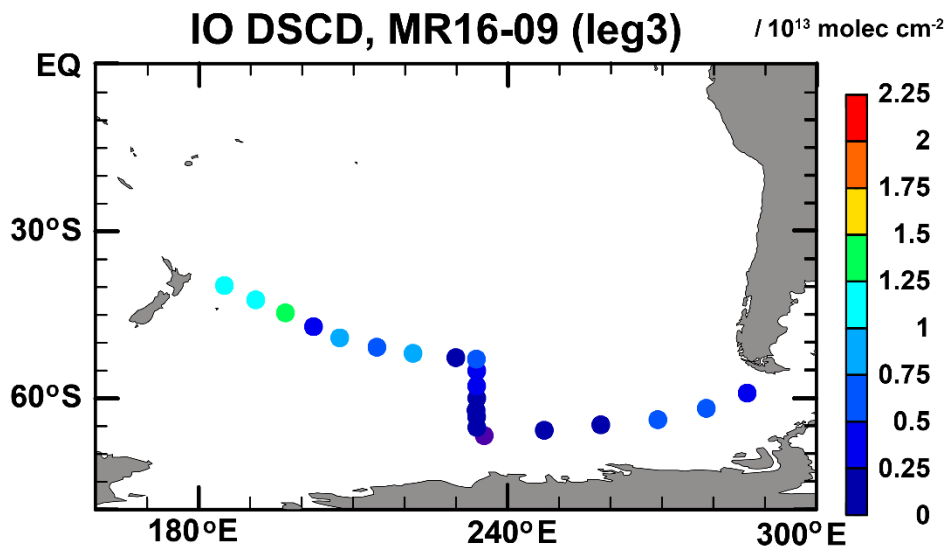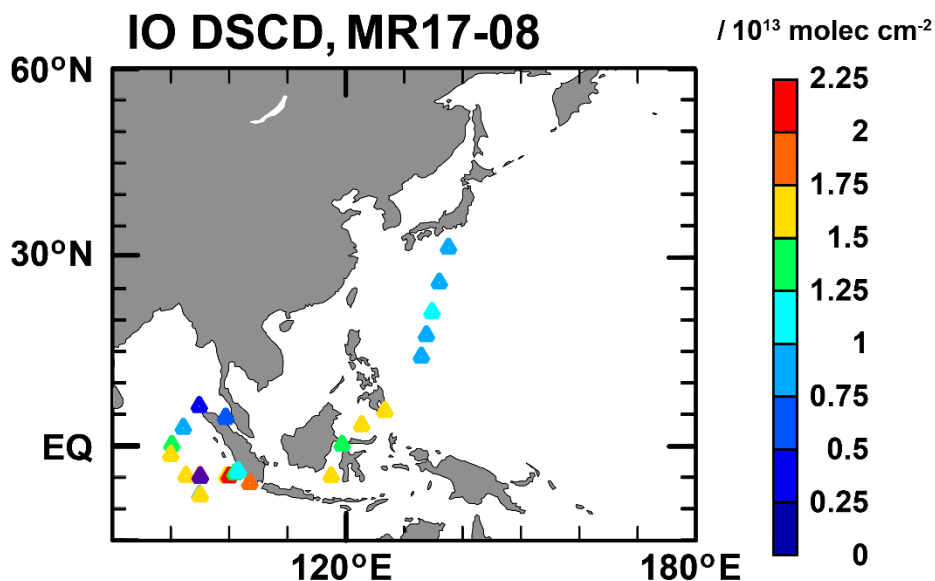
Figure S6: Daily median IO content ((DSCD) for an elevation angle of 3°; molecules cm^{-2}) observed from the R/V *Mirai* for the MR14-06 (leg1), MR15-04, MR15-05, MR16-06, MR16-09 (leg3), MR17-05C, and MR17-08 cruises.

References

Saiz-Lopez, A., Fernandez, R. P., Ordonez, C., Kinnison, D. E., Martin, J. C. G., Lamarque, J. F., and Tilmes, S.: Iodine chemistry in the troposphere and its effect on ozone, Atmos Chem Phys, 14, 13119-13143, 10.5194/acp-14-13119-2014, 2014.

Sekiya, T., Kanaya, Y., Sudo, K., Taketani, F., Iwamoto, Y., Aita, M. N., Yamamoto, A., and Kawamoto, K.: Global Bromine- and Iodine-Mediated Tropospheric Ozone Loss Estimated Using the CHASER Chemical Transport Model, *Sola*, 16, 220-227, 10.2151/sola.2020-037, 2020.